Available online at www.sciencedirect.com
ScienceDirect
International Journal of Thermal Sciences 47 (2008) 742–748
International Journal of Thermal Sciences
www.elsevier.com/locate/ijts

Compounded natural convection enhancement in a vertical parallel-plate channel

Assunta Andreozzi [a,*], Antonio Campo [b], Oronzio Manca [c]

[a] *Dipartimento di Energetica, Termofluidodinamica Applicata e Condizionamenti Ambientali, Università degli Studi di Napoli Federico II, Piazzale Tecchio 80, 80125 Napoli, Italy*

[b] *Department of Mechanical Engineering, The University of Vermont, 33 Colchester Ave., Burlington, VT 05405, USA*

[c] *Dipartimento di Ingegneria Aerospaziale e Meccanica, Seconda Università degli Studi di Napoli, via Roma 29, Aversa (CE) 81031, Italy*

Received 9 October 2006; received in revised form 23 May 2007; accepted 10 June 2007

Available online 27 July 2007

Abstract

This paper addresses the natural convection behavior of air when heated in single vertical, parallel-plate channels. To enhance the heat transfer two passive schemes are combined: (1) an equidistant short plate is inserted at the inlet and (2) two parallel, colinear insulated plates are appended at the exit. The channel plates are symmetrically heated with a uniform heat flux. The computational procedure is made by solving the full elliptic Navier–Stokes and energy equations with the finite-volume methodology in an I-type computational domain that is much larger than the physical domain. Within the framework of a "proof-of-concept" the controlling Grashof number based on the heated plate height ranges between 10^3 and 10^6. The numerical velocity, pressure and temperature fields are post-processed to compute the quantities of engineering interest such as the induced mass flow rate, the pressure at the channel mid-plane and the temperature along the plates. In addition, the Nusselt number and the average Nusselt number, both based on the heated plate height, are presented in graphical form. At the end, optimal channel configurations expressed in terms of the highest average Nusselt number are obtained for the pair of pre-assigned Grashof numbers.

Keywords: Air natural convection; Vertical parallel-plate channel; Equidistant auxiliary plate; Colinear insulated plates; Numerical analysis

Introduction

An extensive amount of research on natural convection heat sinks utilizing vertical, parallel-plate channels has its origins in sub-areas of applied thermal engineering, mostly in electronics cooling and heat exchangers [1].

Natural convection is unquestionably regarded as a very attractive mode of cooling because of its little cost, minimal maintenance and low noise [2]. As reviewed in [1,3], a substantial body of publications has been documented for the specific case of natural convection in vertical parallel-plate channels with symmetric and asymmetric heating conditions employing the parabolic form of the conservation equations. From this collection of studies, the Nusselt number has been traditionally correlated to the modified channel Rayleigh number (sometimes called the Elenbaas–Rayleigh number). The latter is essentially the channel Rayleigh number divided by the aspect ratio of the channel.

Recent interest in heat sinks has centered on the improvement of the limited heat transfer performance when the mode is natural convection [4–6]. Investigations on vertical, parallel-plate channels with colinearly added chimneys and/or auxiliary added plates are infrequent in the literature [3,7–12]. Firstly, the impact of adding a chimney to a single vertical, parallel-plate channel was examined numerically in [13]. Secondly, a finite-difference study dealing with the intensification of natural convection heat transfer from a heated vertical parallel-plate channel to air has been performed in [14]. These authors compared the heat transfer augmentation by inserting an equidistant auxiliary plate at three different elevations inside the channel: (1) at the inlet, (2) at the middle section and (3) at the outlet. It was found that the best location for placing the plate was at the

* Corresponding author. Tel.: +39 081 7682645; fax: +39 081 2390364.
E-mail addresses: assunta.andreozzi@unina.it (A. Andreozzi), acampo@uvm.edu (A. Campo), oronzio.manca@unina2.it (O. Manca).

1290-0729/$ – see front matter
doi:10.1016/j.ijthermalsci.2007.06.013

Nomenclature

a	thermal diffusivity	m^2/s
b	channel gap	m
g	acceleration due to the gravity	m/s^2
Gr	Grashof number, Eq. (4)	
h	auxiliary plate height	m
$h(x)$	convective heat transfer coefficient	$W/m^2\,K$
k	thermal conductivity	$W/m\,K$
L	height of heated plate	m
L_{ext}	height of insulated plate	m
L_{tot}	total channel height	m
L_x	height of the appended reservoir	m
L_y	width of the appended reservoir	m
$Nu(X)$	Nusselt number, Eq. (5)	
Nu	average Nusselt number	
p	pressure	Pa
P	dimensionless pressure, Eq. (4)	
Pr	Prandtl number, Eq. (4)	
$\dot{q}$	wall heat flux	W/m^2
Ra	Rayleigh number, Eq. (4)	
T	temperature	K
u, v	velocity components	m/s
U, V	dimensionless velocity components, Eq. (4)	
x, y	Cartesian coordinates	m
X, Y	dimensionless Cartesian coordinates, Eq. (4)	

Greek symbols

β	volumetric coefficient of expansion	1/K
Δ	difference between two values	
ε	convergence criterion	
η	dummy variable	
ν	kinematic viscosity	m^2/s
θ	dimensionless temperature, Eq. (4)	
ψ	stream function	m^2/s
Ψ	dimensionless stream function, Eq. (4)	
ρ	density	kg/m^3
ω	vorticity	1/s
Ω	dimensionless vorticity, Eq. (4)	

Subscripts

∞	free stream
b	channel gap
L	heated plate height
w	heated plate
$w1$	channel wall
$w2$	mid-plane
max	maximum value

inlet. On the contrary, when the plate was placed at the outlet, it produced an adverse effect. When the plate was placed at the middle section, the outcome was virtually ineffective.

In the treatment of the inflow boundary condition at $X = 0$, a first-order approximation to the pressure drop due to fluid acceleration was devised in [15]. These pioneering findings, when written in dimensionless form, provided the quartet of boundary conditions: $U = U_0$, $V = 0$, $P = -U_0^2/2$ and $\theta = 1$, all at $X = 0$. This choice in turn, facilitated the solution of the governing parabolic conservation equations substantially providing a first-order approximation.

The present paper addresses a practical situation in electronics cooling in which the size of the physical system (a vertical, parallel-plate channel + a colinear chimney) is constrained to a fixed volume. The central goal here is to examine the ramifications associated with the compounded levels of heat transfer intensification in vertical, parallel-plate channels using air in conjunction with two passive schemes: (1) the insertion of a short, auxiliary plate at the inlet and (2) the appendage of colinear insulated plates at the exit (the so-called chimney effect). This "proof-of-concept" study falls short of a parametric study. Perhaps, the resulting elaborate composite channel may find imminent application in rural areas absent of electricity where forced convection air cooling is practically non-existent. From a different perspective, the present study may be conceived as an attempt to estimate the right balance between the control of the maximum wall temperature and an application of a symmetrical wall heat flux. On the other hand, this effort can also be viewed as the maximization of heat transfer density for an assigned volume that is constrained by space limitations. The first objective can be attained by a channel-chimney system that resembles the one analyzed in [16]. The second objective has been brought forward in Refs. [6,11,12,17], and as of late reviewed in [5]. The geometric optimization of L and C-shaped channels involving laminar natural convection was documented in [6]. The objective revolved around the maximization of the heat transfer in the channel. The optimization was performed by the finite element technique in an extended computational domain. In [11] the heat transfer density in laminar forced convection in parallel isothermal blades was maximized. By way of implementing the constructal theory, the spacing between adjacent blades of progressively smaller scales was adjusted in [17]. The same design theory for generating multi-scale structures in a natural convection environment with the objective of maximizing the heat transfer density was investigated in [12]. Here the flow volume was filled with vertical equidistant heated blades of decreasing lengths. Also, a numerical analysis was carried out to compare the results on a global basis.

For the treatment of the conservation equations related to natural convection flows researchers find themselves at a crossroad between a physically-sound elliptic model or the mathematically-ideal parabolic model. The importance of formulating the elliptic model in favor of the parabolic model has been stressed in [18]. In this framework, major discrepancies have been elucidated experimentally for the fully developed limit prevalent in long vertical, parallel-plate channels, reaffirming the fact that the significant axial diffusion phenomena have been neglected in the case of parabolic conservation equa-

tions. Numerical calculations have showed in a convincing manner the pronounced disagreement between the outcomes of the two distinct models, one based on the simplistic parabolic equations and the other on the complete elliptic equations. The present paper paves the way to the discovery of optimal channel configurations represented in terms of the aspect ratio. In other words, this is equivalent to determining the highest average Nusselt number for a fixed Grashof number.

In the present work, a physically-sound elliptic model was preferred to analyze the heat/fluid flow of air inside a vertical parallel-plate channel under the action of symmetric heating with an extended I-shaped domain. The computational domain comprised the actual physical domain (parallel-plate channel with auxiliary plate + chimney) plus two relatively large subdomains, one placed upstream of the channel inlet and the other downstream of the chimney exit.

Numerical results are presented in terms of dimensionless induced mass flow rates, dimensionless pressure profiles along the channel mid-plane, and dimensionless wall temperatures as functions of the aspect ratio b/L and different Grashof numbers. Moreover, Nusselt numbers varying with the dimensionless axial coordinate X pave the way for the calculation of the average Nusselt numbers. Some optimal geometrical configurations have been identified in terms of the channel aspect ratio corresponding to the maximum average Nusselt number. When this information is processed, the end product is the optimal channel configurations emerging at fixed values of the Grashof numbers.

Problem formulation

The geometrical configuration deals with a vertical parallel-plate channel whose plates are uniformly heated with a heat flux strength $\dot{q}$. On one hand, a thin, short and unheated auxiliary plate is placed mid-way between the two parallel plates at the inlet. On the other hand, two colinear insulated plates are attached at the exit. The height of the entire channel is L_{tot}, the heated part of the channel is L and the downstream insulated part is L_{ext}. With the plate separation b and the height of the auxiliary plate h, the physical system is sketched in Fig. 1.

The upward natural convective flow is assumed to be incompressible and laminar. Owing that the physical system is wide along the third coordinate a 2-D approximation is feasible.

Upon defining the stream-function ψ as:

$$\frac{\partial \psi}{\partial y} = u; \qquad \frac{\partial \psi}{\partial x} = -v$$

and the vorticity ω as

$$\omega = \frac{\partial v}{\partial x} - \frac{\partial u}{\partial y}$$

the steady-state Navier–Stokes (accounting for the Boussinesq approximation) and energy equations can be transformed into:

$$\frac{\partial (u\omega)}{\partial x} + \frac{\partial (v\omega)}{\partial y} = \nu \nabla^2 \omega - g\beta \frac{\partial T}{\partial y} \tag{1}$$

$$\frac{\partial^2 \psi}{\partial x^2} + \frac{\partial^2 \psi}{\partial y^2} = -\omega \tag{2}$$

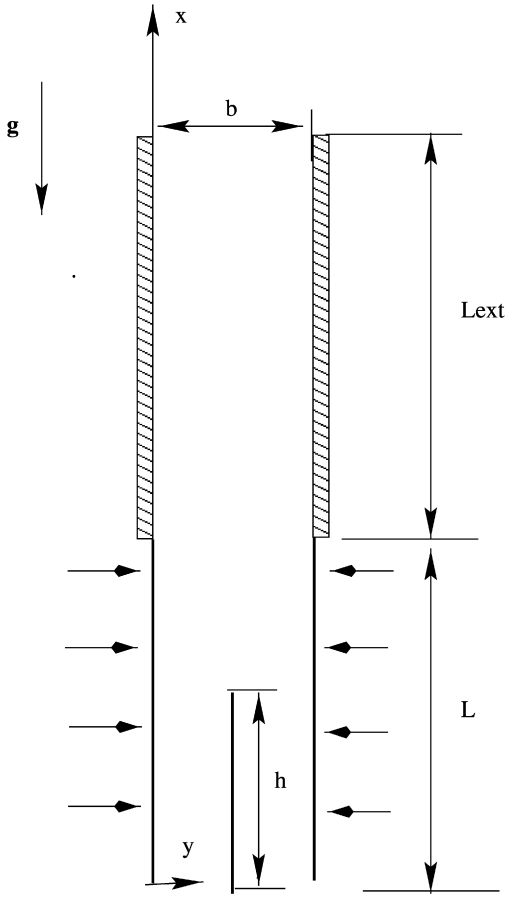

Fig. 1. Partially heated parallel-plate channel.

$$\frac{\partial (uT)}{\partial x} + \frac{\partial (vT)}{\partial y} = a \nabla^2 T \tag{3}$$

The terms involving dissipation and material derivative of pressure in the energy equation (3) are neglected [19].

The participating dimensionless variables and dimensionless groups are defined as:

$$X = x/b, \qquad Y = y/b, \qquad U = ub/\nu, \qquad V = vb/\nu$$
$$P = (p - p_\infty) b^2/(\rho \nu^2), \qquad \theta = k(T - T_\infty)/(\dot{q} b)$$
$$Gr_b = g\beta \dot{q} b^4/(k\nu^2), \qquad Pr = \nu/a, \qquad Ra = Gr_b Pr$$
$$\Psi = \psi/\nu, \qquad \Omega = \omega/(\nu b^2) \tag{4}$$

Numerical solution method

A computational domain of finite dimension illustrated in Fig. 2 is employed to simulate the unconfined airflow that lies far away from the region of thermal disturbance induced by the presence of the two heated parallel plates. As shown in Fig. 2 and due to the existence of geometrical, flow and thermal symmetries, it can be adequately solved in half of the computational domain. The numerical computations were carried out by employing the control volume approach. As suggested in [9,10], the imposed boundary conditions can be rewritten in terms of the stream function and the vorticity to simulate the quasi-infinite domain. When referred to Fig. 2, the boundary conditions are listed sequentially in Table 1.

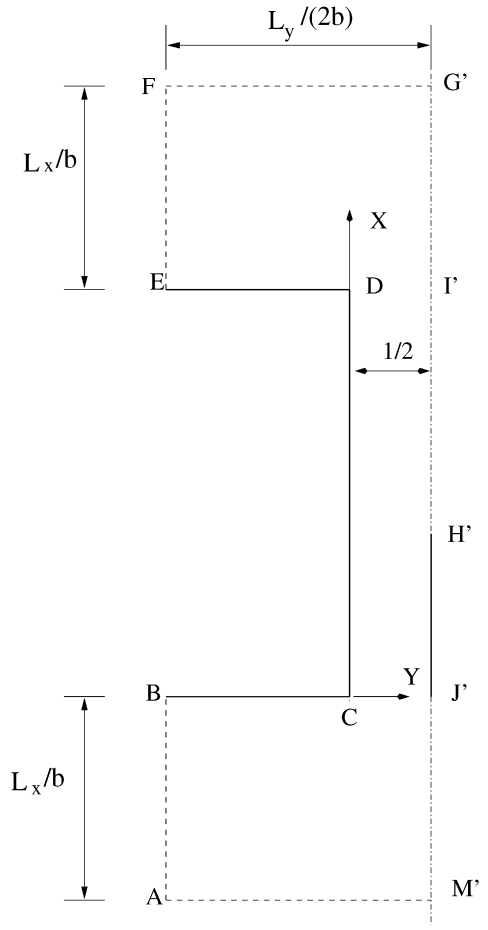

Fig. 2. Computational domain.

Table 1
Boundary conditions related to Fig. 2

ψ	ω	T	Zone
$\frac{\partial^2\psi}{\partial y^2}=0$	$\frac{\partial\omega}{\partial y}=0$	$T=0$	AB
$\frac{\partial^2\psi}{\partial x^2}=0$	$\frac{\partial\omega}{\partial x}=0$	$T=0$	AM'
$\psi=\psi_{w1}$	$\frac{\partial\psi}{\partial x}=0$	$\frac{\partial T}{\partial x}=0$	BC DE
$\psi=\psi_{w1}$	$\frac{\partial\psi}{\partial y}=0$	$-k\frac{\partial T}{\partial y}=\begin{cases}\dot{q}, & \text{heated part}\\ 0, & \text{unheated part}\end{cases}$	CD
$\psi=\psi_{w2}$	$\frac{\partial\psi}{\partial y}=0$	$\frac{\partial T}{\partial y}=0$	$J'H'$
$\frac{\partial^2\psi}{\partial y^2}=0$	$\frac{\partial\omega}{\partial y}=0$	$\frac{\partial T}{\partial y}=0$	EF
$\psi=\psi_{w2}$	$\omega=0$	$\frac{\partial T}{\partial y}=0$	$H'G'$ $M'J'$
$\frac{\partial^2\psi}{\partial x^2}=0$	$\frac{\partial\omega}{\partial x}=0$	$\frac{\partial T}{\partial x}=0$	FG'

The convective heat transfer coefficient $h(x)$, when expressed through the Nusselt number $Nu(X)$, is defined as:

$$Nu(X)=\frac{h(x)b}{k}=\frac{1}{\theta_w(X)} \tag{5}$$

At this stage, we view ourselves at crossroads because two average Nusselt numbers can be formed. One average Nusselt number based on the plates separation b is:

$$Nu_b=\frac{b}{L}\int_0^{L/b} Nu(X)\,\mathrm{d}X \tag{6}$$

In order to evaluate the optimal geometrical configurations in terms of the heated channel aspect ratio b/L or L/b, the characteristic length is the heated plate height L. Accordingly, the modified average Nusselt and Grashof numbers based on L are defined as:

$$Nu_L=\frac{\bar{h}L}{k}\quad\text{and}\quad Gr_L=\frac{g\beta L^4\dot{q}}{k\nu^2} \tag{7}$$

where $\bar{h}$ is the average convective heat transfer coefficient along the channel heated plate. Additionally, linking the modified average Nusselt and the Grashof numbers based on the heated plate height and the average Nusselt and the Grashof number also based on the plate separation yields:

$$Nu_L=\frac{L}{b}Nu_b\quad\text{and}\quad Gr_L=\left(\frac{L}{b}\right)^4 Gr_b \tag{8}$$

Conceptually, the average Nusselt number Nu_L depends on a suitable combination of geometric and thermal quantities. For a specific fluid (fixed Pr), the proper dimensionless functional relation is expressed as:

$$Nu_L=f\left(Gr_L,\frac{b}{L},\frac{h}{L},\frac{L_{\text{ext}}}{L}\right) \tag{9}$$

Once the three quantities Gr_L, h/L and L_{ext}/L are selected, the optimal configuration b/L turns out to be the one with the highest Nu_L value. In this paper, the existence of the optimal channel configuration is pursued for $h/L=0.5$, $L_{\text{ext}}/L=4.0$ and two Grashof numbers: a low 10^3 and a high 10^6. It is worth adding that this similar procedure was employed in previous investigations [3–6,10–12,16,17] because of its usefulness in complex geometries exposed to natural and forced convection.

Realizing that the induced mass flow rate is unknown and the stream function at the channel plate Ψ_{w1} and the mid-plane Ψ_{w2} are not known in advance, the problem is solved with the false transient procedure [20]. The following steps have to be articulated:

1. Assign a guessed $\Delta\Psi$ value, where $\Delta\Psi=\Psi_{w1}-\Psi_{w2}$ represents the induced volumetric flow rate in half of the channel;
2. The ADI technique (Alternating Direction Implicit) transforms the discretized partial differential equations (1)–(3) into a tridiagonal, linear system of algebraic equations. The latter can be solved by the Thomas algorithm;
3. Solve the stream function equation, Eq. (2), by the SLOR method with an optimal relaxation factor of about 1.7;
4. Once Eqs. (1)–(3) are solved, the convergence criteria for the time-like step have to be checked. This is equivalent to saying that the convergence criterion has to be verified at every (i,j) node using:

$$\left|\frac{\eta_{i,j}^{n+1}-\eta_{i,j}^{n}}{\eta_{i,j}^{n+1}}\right|<\varepsilon$$

where η represents either Ω or θ and ε was set equal to 10^{-6};

5. After steady-state conditions are attained, the guessed $\Delta\Psi$ value is verified by integrating the momentum equation along the mid-plane of the channel. This implies that the condition to be verified is:

$$\int_{-L_x/b}^{(L_x+L_{\text{tot}})/b} \frac{\partial P}{\partial X}\,\mathrm{d}X = 0$$

6. If the preceding equation is not satisfied within a pre-set accuracy, say 10^{-2}, return to step 1 and repeat the whole sequential procedure again until a converged solution is obtained.

In order to check the accuracy of the numerical solution, the induced mass flow rate $\Delta\Psi$ and the average Nusselt number Nu are monitored. The idea behind this is to detect any dependency of the numerical solution on the mesh spacing. In this regard, it is observed that doubling the number of nodes along the Y direction from 13 to 27, the two global variables showed a variation of about 1.5%. In addition, a slight dependence of the same variables is evident on the number of nodes along the X direction. In all cases to be analyzed a 27×51 mesh was deemed to be optimal. Moreover, for completeness other tests were carried out to check the dependence of the flow and temperature fields on the dimensions of the two sub-domains. A height equal to twice the heated channel height and a horizontal width equal to twenty one times the channel gap seem to be sufficient to guarantee independent solutions with respect to the dimensions of the two reservoirs.

Discussion of results

Within the framework of a "proof-of-concept", results are reported for air ($Pr = 0.71$) operating at a low $Gr_L = 10^3$ and a high $Gr_L = 10^6$. Typical values of the aspect ratio, b/L, are assigned in the interval [0.1, 1.5]. The extension ratio is set at $L_{\text{tot}}/L = 4$, whereas the ratio of the auxiliary plate height to the heated channel plate one, h/L, is equal to 0.5. The optimal geometrical configurations are evaluated numerically for the aforementioned data values.

Shown in Fig. 3 is the dimensionless mass flow rate, $\Delta\Psi$, as a function of the aspect ratio, b/L, for the two values of Gr_L. When Gr_L increases, a sensible mass flow rate increment is observed; this is clearly caused by a greater driving force. The mass flow rate responds to an increasing function of b/L. This phenomenon can be viewed through either a gain in the driving force or a growth of the channel gap, b. The driving force step up is due to the wall heat flux, because when Gr_L and b are constant, the b/L change is obtained diminishing L. As a consequence a very high $\dot{q}$ value is produced. In contrast, when the channel gap enlarges, it produces a decrease of the pressure losses under the same driving force, $\dot{q}$. Consequently, when the mass flow rate increases, a reduction in the dimensionless maximum wall temperature, $\theta_{w,\max}$, takes place as can

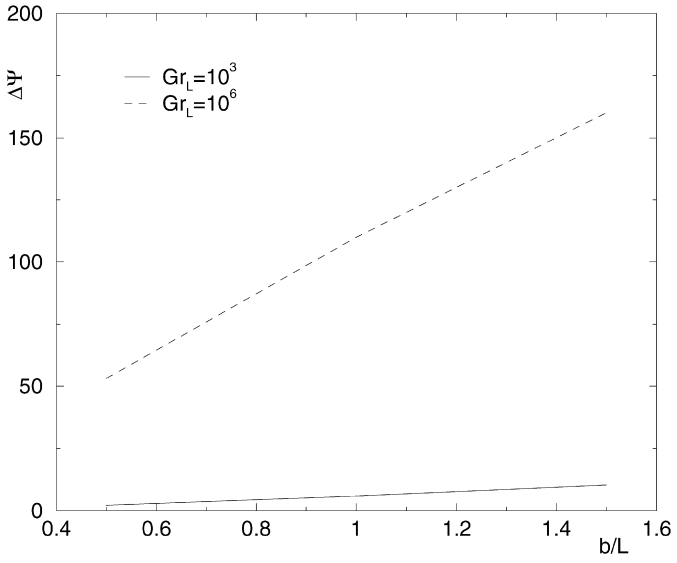

Fig. 3. Dimensionless induced mass flow rate as a function of the aspect ratio for two different Gr_L.

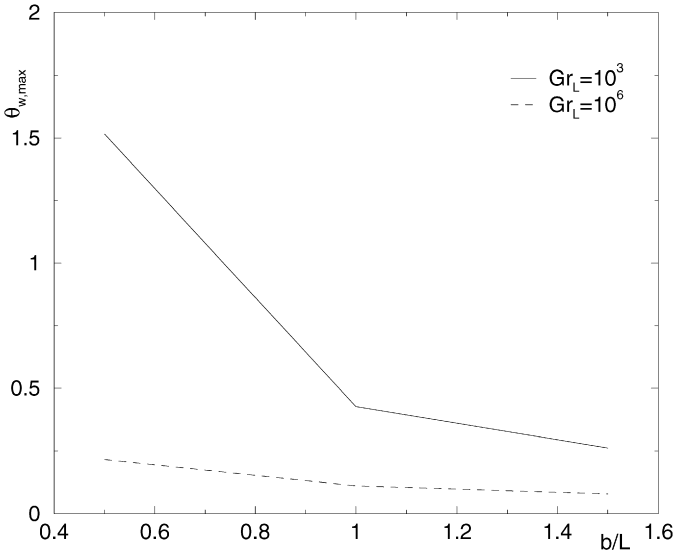

Fig. 4. Maximum heated wall temperatures as a function of the aspect ratio for two different Gr_L.

be confirmed in Fig. 4. In this figure, the maximum wall temperature profiles varying with the aspect ratio, b/L, at $Gr_L = 10^3$ and $Gr_L = 10^6$, are plotted.

Fig. 5 illustrates the Nusselt number values as a function of the axial coordinate X parameterized by the aspect ratio, b/L, at $Gr_L = 10^3$ in Fig. 5(a) and $Gr_L = 10^6$ in Fig. 5(b). At $Gr_L = 10^3$ in Fig. 5(a), the $Nu(X)$ values are higher at higher b/L; this trend is due to the greater mass flow rate that brings along a better heat transfer activity. In fact, the b/L enlargement means either an increase in the channel gap b or a decrease in the heated channel height L. In the first case, it has a bearing on the $Nu(X)$ amplification at least equal to the ratio between b values. Instead, in Fig. 5(b), it is clear that the ratio between the Nusselt number values is greater than the ratio between the b values. This behavior demonstrates that there is a local convec-

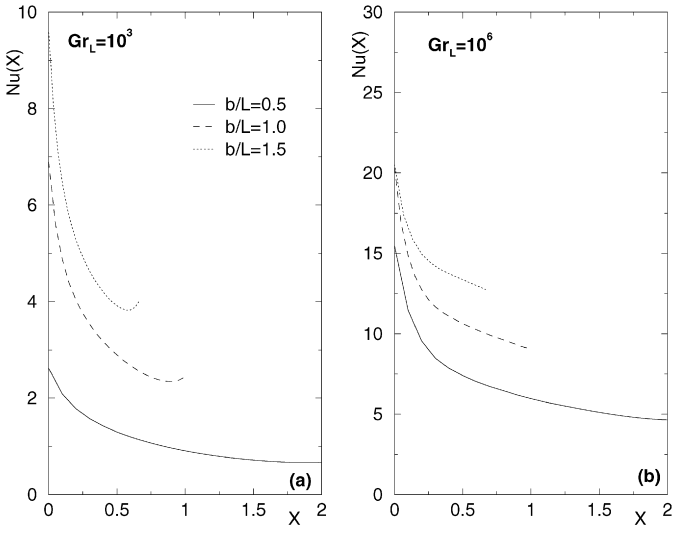

Fig. 5. Axial variation of the Nusselt number for (a) $Gr_L = 10^3$, (b) $Gr_L = 10^6$ and several aspect ratios.

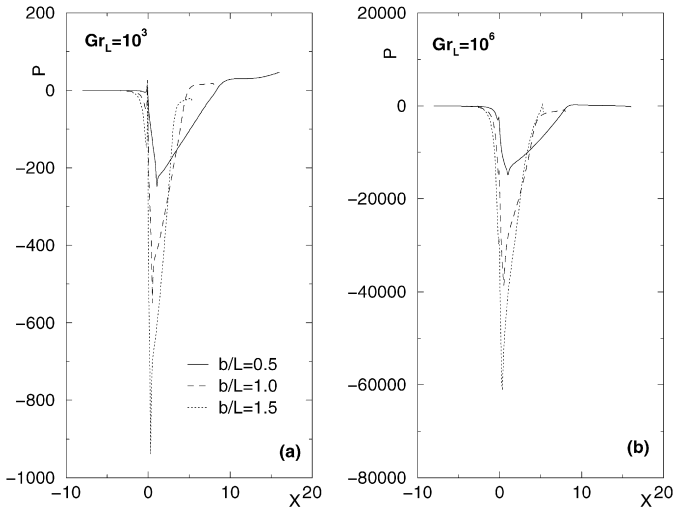

Fig. 6. Mid-plane pressure profiles for (a) $Gr_L = 10^3$, (b) $Gr_L = 10^6$ and several aspect ratios.

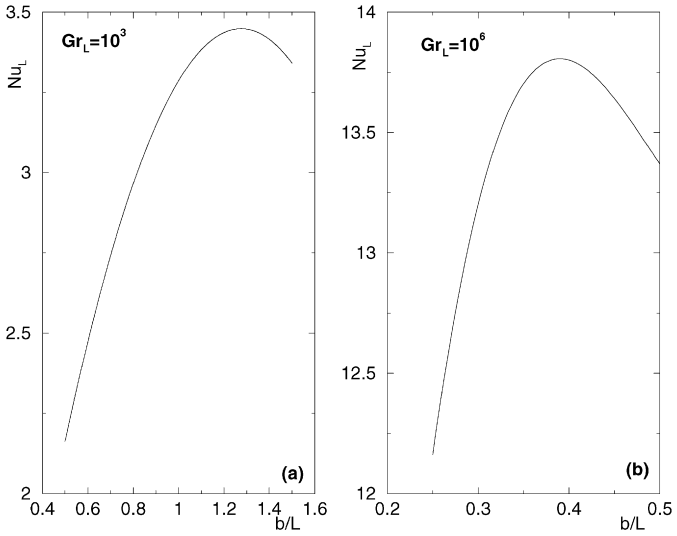

Fig. 7. Average Nusselt number changing with the aspect ratio.

Table 2
Optimal aspect ratios

$(b/L)_{\text{opt}}$	$Gr_L = 10^3$	$Gr_L = 10^6$
Present work	1.27	0.384
[21]	1.21	0.322

tive coefficient expansion, which is produced by an increment in the $\dot{q}/\Delta T$ ratio. In Fig. 5(a) for $Gr_L = 10^3$, it is evident that for $b/L = 1.0$, the $Nu(X)$ profile attains a minimum value, corresponding to the maximum wall temperature value, $\theta_{w,\max}$. Moreover, a subsequent $Nu(X)$ magnification occurs that is responsive to a diminution of the local wall temperature; this behaviour is due to the pronounced diffusive effects with respect to the convective effects at the lowest Gr_L values. The relevance of the diffusive effects causes a diffusive heat transfer with the unheated channel wall. In fact, the shape of the $Nu(X)$ profile in Fig. 5(b) is different because under the prevalent circumstances the convective effects now are of more notoriety than the diffusive effects applicable to $Gr_L = 10^3$.

Portrayed in Fig. 6 collectively are the pressure profiles corresponding to the trio $b/L = 0.5$, 1.0 and 1.5. The pressure profiles linked to $Gr_L = 10^3$ appear in Fig. 6(a) and those linked to $Gr_L = 10^6$ in Fig. 6(b). In agreement with the mass flow rate comportment exhibited in Fig. 3, it is detected that the depression is greater at higher values of b/L. The pressure decreases close to the inlet section, but a small, sharp increase at $X = 0$ is noted where the auxiliary plate is located. This increment is induced by the auxiliary plate leading edge, i.e., the stagnation point for the flow. At the trailing edge of the auxiliary plate the local pressure descends, which is attributed to a flow acceleration produced by the slip condition downstream of the trailing edge. The depression is greater at higher Gr_L; this is stimulated by an increase in the mass flow rate.

Fig. 7 displays the susceptibility of the average Nusselt number, Nu_L, to changes in the aspect ratio b/L for the two Gr_L investigated. Here, it is observed that, for the two Gr_L values, the Nu_L profile climbs up to a maximum value. This tendency is indicative of an optimal geometrical configuration, which entails to a better heat transfer. Further, it is important to observe in the items of Table 2 that, for this kind of configurations, the optimal b/L values are slightly higher than the ones obtained in [21].

Conclusions

A numerical analysis of a heated vertical parallel-plate channel owing an auxiliary plate at the inlet and two insulated extension plates attached to the heated walls at the exit has been carried out. The numerical approach established the existence of optimal geometrical configurations. To perform the analysis, air was placed in an expanded I-type computational domain. The rationale for this was to capture the diffusion phenomena by momentum and energy that could occur upstream and downstream of the channel. The mass flow rate was found to vary proportionally with the Grashof number based on the

heated plate height L and the heated channel aspect ratio b/L. In agreement with this, the maximum wall temperature diminishes with increments in b/L and Gr_L. The Nusselt number ascends when the heated channel aspect ratio increases; this connection is due to the greater mass flow rate. The mass flow rate augmentation has been underlined through the centerline pressure profiles accounting for the auxiliary plate; in fact, the pressure peaks are due to the velocity alterations. The insertion of an auxiliary plate and the appendage of two insulated plate extensions furnishes optimal channel configurations. This translates into the maximization of the convective heat transfer with slightly higher b/L values with respect to those for the bare channel [21].

The next phase of the analysis will seek an enlarged range of geometrical and thermal parameters in order to evaluate the optimal configurations within the perspective of a parametric study. Moreover, the effect of heat conduction in the heated channel walls and the auxiliary plate and radiative heat transfer should be analyzed to determine the thermal and the fluid dynamic behaviors and to evaluate the optimal geometrical configurations. Another interesting configuration could be the packaging of parallel channel-chimney.

Acknowledgement

This research project was supported by the MIUR with the grant PRIN 2005-2007.

References

[1] O. Manca, B. Morrone, S. Nardini, V. Naso, Natural convection in open channels, in: B. Sunden, G. Comini (Eds.), Computational Analysis of Convection Heat Transfer, WIT Press, Southampton, UK, 2000, pp. 235–278.

[2] G.P. Peterson, A. Ortega, Thermal control of electronic equipment and devices, in: Advances in Heat Transfer, vol. 20, Academic Press, New York, 1990, pp. 181–314.

[3] A. Campo, O. Manca, B. Morrone, Numerical analysis of partially heated vertical parallel plates in natural convective cooling, Numer. Heat Transfer, Part A 36 (1999) 129–151.

[4] G.A. Ledezma, A. Bejan, Optimal geometric arrangement of staggered vertical plates in natural convection, J. Heat Transfer 119 (1997) 700–708.

[5] A.K. da Silva, S. Lorente, A. Bejan, Constructal multi-scale structures for maximal heat transfer density, Energy 31 (2006) 620–635.

[6] A.K. da Silva, L. Gosselin, Optimal geometry of L- and C-shaped channels for maximum heat transfer rate in natural convection, Int. J. Heat Mass Transfer 48 (2005) 609–620.

[7] C.H. Cheng, W.H. Huang, H.S. Kou, Laminar free convection of the mixing flows in vertical channels, Numer. Heat Transfer 14 (1988) 447–463.

[8] K. Lee, Natural convection on vertical parallel plates with an unheated entry or unheated exit, Numer. Heat Transfer, Part A 25 (1994) 477–493.

[9] A. Andreozzi, O. Manca, Thermal and fluid dynamic behaviour of symmetrically heated vertical channels with auxiliary plate, Int. J. Heat Fluid Flow 22 (2001) 424–432.

[10] A. Andreozzi, O. Manca, V. Naso, Natural convection in vertical channels with an auxiliary plate, Int. J. Numer. Methods Heat Fluid Flow 12 (6) (2002) 716–734.

[11] A. Bejan, Y. Fautrelle, Constructal multi-scale structure for maximal heat transfer density, Acta Mech. 163 (2003) 39–49.

[12] A.K. da Silva, A. Bejan, Constructal multi-scale structure for maximal heat transfer density in natural convection, Int. J. Heat Fluid Flow 26 (2005) 34–44.

[13] P.H. Oosthuizen, A numerical study of laminar free convective flow through a vertical open partially heated plane duct, ASME HTD 32 (1984) 41–48.

[14] T. Aihara, T. Ohara, A. Sasago, M. Ukaku, F. Gori, Augmentation of free-convection heat transfer between vertical parallel plates by inserting an auxiliary plate, in: Proceedings of the 2nd European Thermal Sciences Conference Rome, Italy, 1996.

[15] T. Aihara, Effects of inlet boundary conditions on numerical solutions of free convection between vertical parallel plates, Reports Inst. High Speed, Tohoku University, Sendai, Japan 28 (1973) 1–27.

[16] A. Andreozzi, B. Buonomo, O. Manca, Numerical study of natural convection in vertical channels with adiabatic extensions downstream, Numer. Heat Transfer, Part A 47 (2005) 741–762.

[17] A. Bejan, Shape and Structure, from Engineering to Nature, Cambridge University Press, Cambridge, UK, 2000.

[18] O. Manca, B. Morrone, V. Naso, A Numerical study of natural convection between symmetrically heated vertical parallel plates, in: Atti del XII Congresso Nazionale UIT, L'Aquila, Italy, 1994, pp. 379–390.

[19] B. Gebhart, Y. Jaluria, R. Mahajan, B. Sammakia, Buoyancy-Induced Flows and Transport, Hemisphere Publishing Co., Washington, DC, 1988.

[20] P.J. Roache, Fundamentals of Computational Fluid Dynamics, Hermosa Publishers, Albuquerque, NM, 1998.

[21] B. Morrone, A. Campo, O. Manca, Optimum plate separation in vertical parallel-plate channels for natural convective flows: incorporation of large spaces at the channel extremes, Int. J. Heat Mass Transfer 40 (1997) 993–1000.